ChemPubSoc Europe

DOI: 10.1002/cssc.201501023

CHEMSUSCHEM Full Papers

Solar Thermochemical Energy Storage Through Carbonation Cycles of $SrCO_3$/SrO Supported on $SrZrO_3$

Nathan R. Rhodes,[a] Amey Barde,[a] Kelvin Randhir,[a] Like Li,[a] David W. Hahn,[a] Renwei Mei,[a] James F. Klausner,[a] and Nick AuYeung*[b]

Solar thermochemical energy storage has enormous potential for enabling cost-effective concentrated solar power (CSP). A thermochemical storage system based on a SrO/$SrCO_3$ carbonation cycle offers the ability to store and release high temperature (≈1200 °C) heat. The energy density of $SrCO_3$/SrO systems supported by zirconia-based sintering inhibitors was investigated for 15 cycles of exothermic carbonation at 1150 °C followed by decomposition at 1235 °C. A sample with 40 wt% of SrO supported by yttria-stabilized zirconia (YSZ) shows good energy storage stability at 1450 MJ m^{-3} over fifteen cycles at the same cycling temperatures. After further testing over 45 cycles, a decrease in energy storage capacity to 1260 MJ m^{-3} is observed during the final cycle. The decrease is due to slowing carbonation kinetics, and the original value of energy density may be obtained by lengthening the carbonation steps.

Introduction

Concentrated solar power (CSP) generation combined with energy storage has the intrinsic advantage of dispatchability, which is the ability to provide energy upon demand, or alternatively, store energy when there is no demand. Despite this advantage, a transformational breakthrough is needed in the area of energy storage to make CSP competitive with photovoltaics or conventional fossil power sources. Thermochemical storage essentially allows for storage of concentrated solar energy by conversion to chemical energy at greater volumetric densities than sensible or latent heat methods, reducing the physical footprint of CSP systems and the necessary capital investment. The ideal thermochemical system consists of a reversible reaction where a high-temperature, solar-driven endothermic reaction can be performed during daylight hours, allowing for heat release upon the reverse, exothermic reaction during times of high demand. The greater the temperature of this energy release, the greater the potential for high efficiency power generation. This work shows the promising potential of a high temperature carbonate thermochemical energy storage scheme.

Although photovoltaic cells convert solar energy directly to electricity, effective utilization of this generated electricity at large scales requires electricity energy storage. In contrast, CSP converts solar energy to heat before transformation to electrical energy, potentially allowing for more cost-effective storage. A CSP plant with storage offers dispatchable renewable power, allowing for high plant utilization because it can provide energy for load shifting or spinning reserves—essentially power on demand. Although promising, thermal energy storage subsystems are often cost prohibitive. Greater volumetric energy storage density is therefore desired to bring down capital costs. Thermochemical energy storage (TCES) offers a potential route to achieving a ten-fold increase in energy storage density over sensible or latent heat thermal energy storage methods.[1]

TCES of high temperature thermal energy features a solar endothermic decomposition reaction followed by an exothermic formation reaction. An important characteristic is that the reaction can go forward or backward within a reasonable temperature range attainable by solar thermal energy. Candidate species for decomposition include oxides, hydrides, hydrates, sulfates, and carbonates.[2] Considerable work has also been carried out on ammonia dissociation[3] and sulfur disproportionation followed by combustion.[4]

Perhaps the most elegant design of a TCES subsystem to date is the coupling of high and low temperature metal hydrides. A high temperature metal hydride is defined as a metal hydride that decomposes at temperatures greater than 400 °C while the low temperature metal hydride can easily decompose at or near room temperature using either mild pressure or temperature swing. Harries et al. introduced a pathway where H_2 is released from thermal decomposition of a high-temperature metal hydride such as CaH_2 (decomposition ca. 950 °C) and stored in a hydrogen reservoir of low temperature metal hydrides until equilibrium is reached.[5] Recently, $NaMgH_2F$ was shown to have 1416 kJ kg^{-1} of practical energy storage (approximately 1968 MJ m^{-3}) at a decomposition tem-

[a] N. R. Rhodes, Dr. A. Barde, K. Randhir, Dr. L. Li, Dr. D. W. Hahn, Dr. R. Mei, Dr. J. F. Klausner
Department of Mechanical and Aerospace Engineering
University of Florida
Gainesville, FL 32611 (USA)

[b] Dr. N. AuYeung
School of Chemical, Biological and Environmental Engineering
Oregon State University
Corvalis, OR 97331 (USA)

Supporting Information and ORCID(s) from the author(s) for this article are available on the WWW under http://dx.doi.org/10.1002/cssc.201501023.

perature of 478 °C. A technoeconomic analysis revealed that the overwhelming cost driver for this technology is the low-temperature metal hydride.[6]

Carbonates are especially attractive because of their low cost and high global abundance. Carbonation/decomposition cycling using $CaCO_3$/CaO has been heavily explored for both energy storage[7–13] and carbon-capture purposes.[14–28] The drawback to CaO/$CaCO_3$ is the decrease in reactivity during the carbonation reaction as the capacity for CaO to take up CO_2 is significantly diminished over multiple cycles to roughly one third of the theoretical value.[2] Compounds such as $CaCO_3$ and $BaCO_3$ have been investigated for both energy storage and carbon capture/release applications; however, both compounds show loss of reactivity after cycling, which is not acceptable for robust integration with a CSP plant.[13,18,27,29]

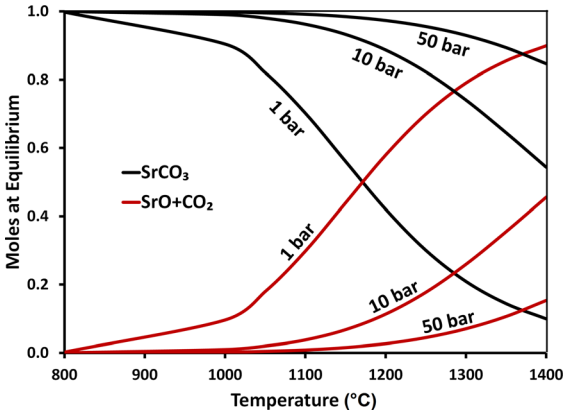

Figure 1. Equilibrium curves for a system with initial feed of 1 mol $SrCO_3$ at 1, 10, and 50 bar.

Thermodynamics

As the efficiency of a heat engine increases with the upper operating temperature, it is imperative that a thermochemical storage system has the ability to operate at temperatures as high as attainable using state-of-the-art solar concentration methods. The use of $SrCO_3$ for energy storage has been previously introduced by Arlt and Wasserscheid in 2011.[30] The energy storage scheme is based on the cyclical carbonation/decarbonation of a SrO/$SrCO_3$ system:

$$SrCO_3 \rightleftharpoons SrO + CO_2 \qquad \Delta H^\circ_{rxn,\,25\,^\circ C} = 234\ kJ\,mol^{-1} \qquad (1)$$

During the solar-driven endothermic step, $SrCO_3$ is decomposed, releasing CO_2 to storage. During times of power generation, CO_2 is released from storage back to the high temperature receiver/reactor where the reverse, exothermic reaction takes place and heat is transferred to a power block. The high, yet attainable decomposition temperature ($\Delta G^\circ = 0$ kJ mol^{-1} at 1175 °C) at which the system reaches chemical equilibrium bodes well for generating high-temperature thermal energy upon carbonation of SrO—a quality that is lacking in most proposed TCES subsystems.

The thermodynamics of the reversible reaction are favorable in both directions within a temperature range amenable to solar thermal concentration. Figure 1 shows the variation of the equilibrium $SrCO_3$ and SrO + CO_2 values on a basis of 1 mol $SrCO_3$ using a Gibbs minimization scheme at several pressures. It should be noted that there are no significant side reactions or side products. Thermal decomposition is shown to occur at upper limit temperatures attainable by the central tower (i.e., < 1300 °C). If decomposition occurs under atmospheric pressure (1 bar) at a temperature of 1300 °C and it is assumed that the carbonation tends to completion at a pressure of 10 bar, the extent of reaction achieved in the simulated closed system may exceed 75%. This extent of reaction represents roughly 175 kJ mol^{-1} under normal conditions or approximately 1700 kJ kg_{SrO}^{-1}.

The thermodynamics of the system highly depend on the partial pressure of CO_2, which is the total system pressure as CO_2 is the only gas in the system. As CO_2 is released from the high-temperature decomposition reaction, gas evolves and contributes to increasing the total system pressure, eventually reaching chemical equilibrium in a closed system. To delay the pressure increase and the corresponding equilibrium, CO_2 should be sent to external storage. As more energy may be available during the higher-temperature decomposition step (during sun exposure), compression of evolved CO_2 may be more feasible. During carbonation, higher pressures will be beneficial to increase the extent of reaction. If CO_2 is stored at higher pressure, it will also decrease the storage volume required, potentially decreasing the capital costs. Furthermore, unlike metal hydride TCES systems that involve flow and storage of H_2, CO_2 is neither explosive—a trait that becomes increasingly important when considering safety measures in scale up—nor does it cause embrittlement of pipes or storage vessels, which is important in achieving a 30 year subsystem lifetime.

Kinetics and longevity

The decomposition step alone has been well studied as $SrCO_3$ is a model compound for thermal analysis.[31,32] However, what is less known is the ability of CO_2 to repeatedly carbonate the SrO to a high extent of reaction. The high temperatures involved cause sintering and loss of surface area, which lead to slowing of kinetics over time. This problem is not unique to the carbonation of SrO; carbonation of CaO has faced similar problems of sintering and pore clogging.[28] An innovative and extremely promising solution was introduced by Zhao et al., which involved the addition of a polymorphic spacer material (Ca_2SiO_4) that undergoes volumetric expansion as a result of a phase change upon cooling from 800 to 650 °C.[14] The volumetric expansion allows regeneration of surface area in the particle bed. The researchers were able to achieve nearly full conversion (97%) of CaO to $CaCO_3$ with addition of 30 wt% Ca_2SiO_4 for 15 consecutive carbonation/decomposition cycles. Valverde et al. have recently successfully recovered the carbonation reactivity of CaO in two successive carbonation steps.[33] The second "recarbonation" step is conducted at an elevated temperature and is shown to significantly recover reactivity

after ten cycles without recarbonation. The group theorized that thermal fatigue induced during recarbonation may lead to internal stress and rupture in the material, leading to enhanced diffusion of CO_2 into the bulk CaO.

Other approaches include creating porous structures or mixing reactive material with an inert support. Sacrificial pore formation has been used successfully to create porous metal oxide structures that facilitate gas–solid reactions at even higher temperatures for other solar thermochemical applications.[34,35] Inert supports with melting temperatures in excess of the reactive material have been shown to help alleviate the effects of sintering and may lead to increased reactivity stability over many cycles.[36,37]

Results and Discussion

Table 1 details the individual specimens used in this study. $SrZrO_3$ and yttria-stabilized strontium zirconate (SrYSZ) are the two investigated inert support materials. Samples are labeled according to their intended SrO and support material content. That is, 40% SrO w/$SrZrO_3$ corresponds to a sample with an intended SrO/$SrZrO_3$ mass ratio of 2:3. During synthesis and storage prior to experimentation, sample stocks were inevitably exposed to a degree of ambient moisture resulting in partial hydration of SrO. This leads to an actual SrO content that may differ slightly from the intended value. Mass loss during the dehydration step at 1100 °C is assumed to be due to H_2O loss and is used to estimate the true SrO content listed in Table 1 prior to cycling. Each sample is prepared with particle diameters in the range of 38–63 μm for both SrO and support material.

Table 1. Support materials and SrO content (wt%) of specimens.

Sample name	SrO content [wt%]
50% SrO w/SrYSZ	50.6
40% SrO w/SrYSZ	39.7
50% SrO w/$SrZrO_3$	48.3
40% SrO w/$SrZrO_3$	37.9

The most telling metric for comparing the performance of these materials is volumetric energy density. In a real system, a reactor will be more productive if it contains more mass of a denser material with similar or even less productivity per gram. Thus, materials with similar % mass change observed in thermogravimetry (TG) may not be truly comparable if one exhibits a greater density. Energy density for a given cycle is calculated using Equation (2):

$$\text{Energy density}[\text{MJ m}^{-3}] = \frac{\Delta m \cdot \rho \cdot \Delta H^{\circ}_{rxn,\,25\,^{\circ}\text{C}}}{M_{CO_2} \cdot m_i} \quad (2)$$

Sample density, ρ, is estimated using the measured post-experimental height, diameter, and mass. Δm is the mass change observed by the TG for a given cycle and is taken as the total CO_2 uptake. Mass of the demoisturized sample is represented by m_i. Table 2 summarizes the apparent density of each sample used to calculate the energy density along with the % mass change observed in TG during the tenth cycle.

Figure 2 shows the energy density for each cycle of the supported SrO samples. Samples with 40% reactive SrO content, though exhibiting less initial reactivity, demonstrate extremely repeatable cyclic energy density. The sample of 40% SrO w/$SrZrO_3$ features stability at approximately 1030 MJ m^{-3}, whereas that of 40% SrO w/SrYSZ exhibits a greater energy density equilibrium point of nearly 1450 MJ m^{-3}. For both support materials, initial mass change increases with SrO content. The effect of sintering is observed in both samples with 50% SrO although degradation associated with the SrYSZ-supported sample is more aggressive. 50% SrO w/SrYSZ exhibits approximately 1850 MJ m^{-3} during the tenth cycle, a decrease of 32% from the initial cycle. 50% SrO w/$SrZrO_3$ also degrades, down 9% from its peak energy density to nearly 1600 MJ m^{-3} by cycle ten. The greater density of 50% SrO samples leads to a larger energy density per milligram of mass change. However, degradation of these samples is such that ultimate stability is likely not fully realized after ten cycles.

Table 2. Measured density and % mass change observed using TG for $SrZrO_3$-supported SrO specimens.

Sample	Apparent density [kg m^{-3}] (±5%)	Mass change: 10th cycle [%] (±0.1%)
50% SrO w/SrYSZ	2380	14.6
40% SrO w/SrYSZ	1620	16.7
50% SrO w/$SrZrO_3$	2400	12.5
40% SrO w/$SrZrO_3$	1800	10.9

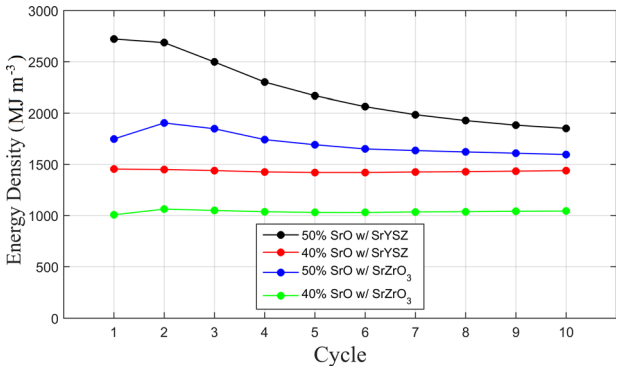

Figure 2. Energy density of supported SrO specimens over ten cycles.

For reference, Table 3 lists the maximum theoretical energy densities for samples with a range of SrO content. These figures correspond to zero porosity or a theoretically solid sample that has achieved complete conversion to $SrCO_3$. SrO contents of 40% and 50% that correspond to the active portions of tested samples are included. The theoretical maximum values are much greater than those realized in Figure 2, lead-

Table 3. Maximum theoretical energy density for a range of SrO content and zero porosity.

SrO Content [wt%]	Maximum theoretical energy density [MJ m^{-3}]
100	10614
50	5307
40	4246

ing to the conclusion that a significant amount of material had not reacted.

Given that 40% SrO w/SrYSZ exhibits the greatest stable energy density over ten cycles, it was chosen for further investigation. Figure 3 shows representative TG mass change data for a single set of fifteen cycles. To show repeatability, Figure 4 plots the average energy density from three identical sets of

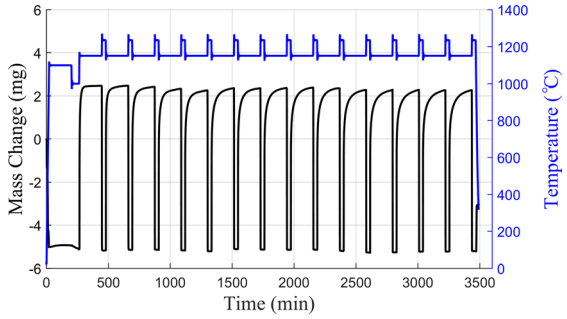

Figure 3. Mass change vs. temperature TG data for a single set of fifteen cycles with 40% SrO w/SrYSZ.

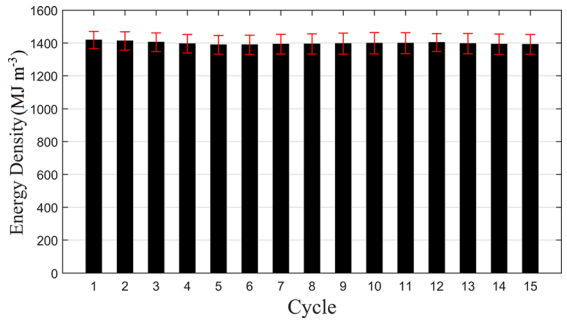

Figure 4. Average energy density ±1 standard deviation for three fifteen-cycle experiments for 40% SrO w/SrYSZ.

fifteen cycles for 40% SrO w/SrYSZ. The energy density is extremely stable at approximately 1400±60 MJ m^{-3} over fifteen cycles. This comparatively small error is evidence of high repeatability for 40% SrO w/SrYSZ. The average energy density for 50% SrO w/SrYSZ is shown in Figure S3 of the Supporting Information.

To test the extended stability of 40% SrO w/SrYSZ, 45 cycles were conducted identically to the previously run cycles. The energy density for each cycle is shown in Figure 5. As shown in Figures 3 and 4, stability is observed for the first fifteen cycles at an energy density of approximately 1430 MJ m^{-3}.

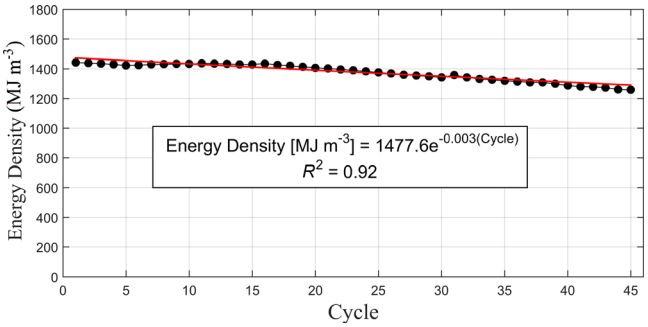

Figure 5. Energy density over 45 cycles for 40% SrO w/SrYSZ.

Thereafter, a slight decrease in energy density is observed with additional cycles, down to 1260 MJ m^{-3} during cycle 45. An exponential fit to cyclic energy density data yields an empirical relationship between energy density and cycle number, N, with R^2 of approximately 0.92 [Eq. (3)]:

$$\text{Energy density}[\text{MJ m}^{-3}] = 1477\exp(-0.003\,N) \quad (3)$$

Similar energy density data and discussion for 101 cycles with 50% SrO w/SrYSZ can be found in Figures S4 and S5 of the Supporting Information.

The mass change profiles of cycles 1 and 45 have been superimposed in Figure 6 for better visualization. Comparison of these curves reveals two apparent kinetic regimes during the carbonation step. The first is an aggressive regime that occurs very quickly, attributed to the carbonation reaction primarily on the surface of the sample. A second, slower regime is later observed as a $SrCO_3$ layer forms on the surface and CO_2 must diffuse through this layer to further carbonate the sample. The

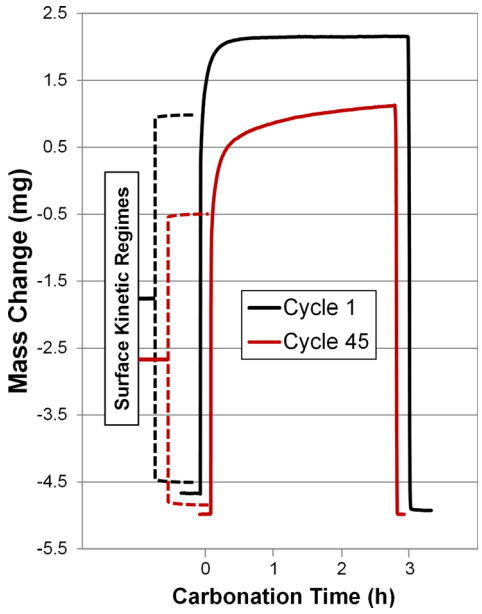

Figure 6. Comparison of TG mass change curves of the first and last cycles from the 45-cycle 40% SrO w/SrYSZ experiment. The curve for cycle 45 is offset for clarity.

first cycle consists almost completely of the surface regime and quickly reaches a maximum degree of carbonation. As the sample is cycled, sintering decreases the sample's surface area and reduces the extent of the surface regime. Consequently, each additional cycle is composed of the slower diffusion regime. Cyclic energy density subsequently falls as the maximum carbonation degree is no longer achieved in the allotted time for carbonation. The initial stable level of energy density may be recoverable given a longer time for carbonation for later cycles.

Conclusions

Samples of SrO with inert support material of yttria-stabilized strontium zirconate (SrYSZ) and $SrZrO_3$ have both energy densities exceeding 1500 MJ m^{-3} for ten cycles at temperatures not previously approached by other thermochemical energy storage (TCES) systems. The high-temperature nature of this TCES concept could potentially power a solar-driven combined cycle power plant at times of no solar input. Comparing similar samples with differing SrO content demonstrates that sintering begins to hamper the reactive stability as the SrO content surpasses at least 38% by mass in the $SrZrO_3$ support material and 40% in SrYSZ. Although the effect of sintering is evident in samples containing 48–50% SrO by mass, a threshold of reactive equilibrium, as noted above, is observed for specimens with less SrO content. For both materials with 40% and 50% SrO, those supported on SrYSZ exhibit greater mass change and energy density than samples with $SrZrO_3$ as support. This observation leads to the initial conclusion that SrYSZ may be superior to $SrZrO_3$ as a support material for SrO under the tested conditions.

A 45-cycle test of 40% SrO w/SrYSZ was conducted to further test the extent of the observed stability. The energy density decreased after fifteen cycles from 1430 MJ m^{-3} in the first cycle to approximately 1260 MJ m^{-3} after 45 cycles. Inspection of mass change profiles reveals the presence of two primary kinetic regimes during carbonation. The first, a quick surface regime, is responsible for the majority of the observed energy density. The diffusion regime proceeds more slowly, likely because of the need of CO_2 to diffuse through the earlier formed $SrCO_3$ surface layer. As the sample is subjected to more cycles, the degree of contribution during the surface regime is reduced and the carbonation extent becomes increasingly reliant on diffusion. Slowing reaction rates leads to a lack of recovery of the previously achieved energy density. At the end of the 45th cycle, carbonation is not yet complete. An increased degree of energy storage could be achieved given a longer time for carbonation.

Ideally, there exists an ideal SrO content that will maintain the greatest stable value of energy density over many cycles for each supportive material. There are many additional parameters (e.g., temperature and pressure) that have not yet been fully explored. Optimization of SrO content, particle size (for both SrO and support) beyond 38–63 μm, and orientation of SrO and support particles during synthesis may aid in the pursuit of an ideal supported SrO material. Additionally, more sophisticated methods of synthesis (e.g., wet methods such as co-precipitation) may result in a more homogeneously supported material with greater stability.

Experimental Section

Strontium oxide (Alfa Aesar) and 8 mol% yttria-stabilized zirconia (YSZ) (99.9%, Advanced Materials) were mixed well at a 1:1 molar ratio. The mixture was heated in a muffle furnace at 1500 °C for 8 h under air. During this process, yttria-stabilized strontium zirconate (SrYSZ) was synthesized through a solid-state reaction between strontium oxide and YSZ. SrYSZ powder was sieved to prepare samples in different size ranges: 25–38, 38–63, 63–106, and 106–125 μm. Strontium zirconate without yttria ($SrZrO_3$) was also prepared as a support material.

To confirm formation of SrYSZ, Raman spectra were recorded using a dispersive micro-Raman spectrometer (JY Horiba LabRam, 632 nm excitation). As no standard for SrYSZ was available, our synthesized SrYSZ was compared to standards for $SrZrO_3$ and SrO. Figure 7 shows prominent peaks for both the $SrZrO_3$ standard and

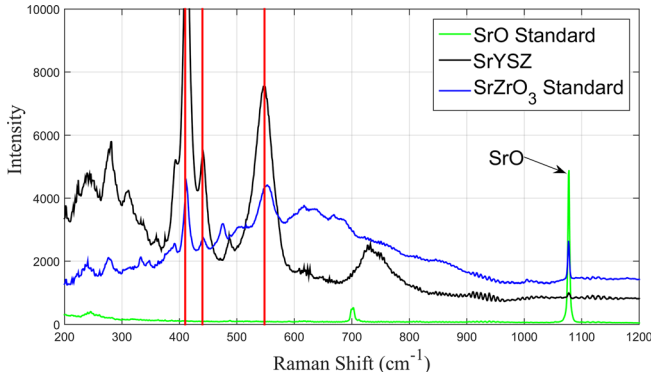

Figure 7. Raman spectra of SrO and $SrZrO_3$ standards against synthesized SrYSZ. Peaks shared by SrYSZ and the $SrZrO_3$ standard (410, 440, and 548 cm^{-1}) are noted with red lines.

SrYSZ at approximately 410, 440, and 548 cm^{-1}. Other significant peaks are also present: most notable is a SrYSZ peak at 730 cm^{-1} not seen in the $SrZrO_3$ standard. We attributed these differing peaks to the influence of yttria in the synthesized sample. A standard for SrO is also included, the peak of which is located at 1078 cm^{-1}. Peaks at this point in the other spectra are likely from traces of unreacted SrO from synthesis. Spectra for selected experimental samples are shown in Figures S1 and S2 in the Supporting Information.

SrO is highly hygroscopic in nature and transforms into $Sr(OH)_2$ and later $Sr(OH)_2{\cdot}8H_2O$ by absorbing moisture from air. It is difficult to protect SrO from the moisture during the material synthesis process and some SrO is likely to form $Sr(OH)_2$ or a hydrate. Thus, a starting material for the experimental investigation is likely a mixture of SrO and $Sr(OH)_2$ with unknown mass ratio of constituent materials. To avoid this ambiguity, each sample was prepared using powders that had been left open to the atmosphere for 72 h. During the initial heat treatment, $Sr(OH)_2$ lost moisture and SrO was recovered. SrO was heat-treated at similar conditions described earlier in this section for synthesis of strontium zirconate. The sintered structure of SrO was exposed to air at room temperature for 72 h. The resulting powder was sieved to prepare samples

in different particle size ranges: 25–38, 38–63, 63–106, and 106–125 μm. The theory for determination of the mass ratio of the support material to the reactive material for experimental samples is detailed in the Supporting Information.

Data were obtained by performing thermogravimetric analysis (TGA) using a Netzsch STA 449 F3 Jupiter TG. Approximately 50 mg of material was measured into an alumina crucible for experimentation. Before cycling began, supported SrO specimens were subjected to heat treatment at 1100 °C for 3 h under an inert atmosphere (Ar) so that any latent $Sr(OH)_2$ or $SrCO_3$ formed from exposure to air could be decomposed to SrO. Specimens were then exposed to a singular flow of 120 mL min^{-1} of CO_2 at 1150 °C for 3 h during which time the exothermic carbonation reaction occurred. Immediately following carbonation, the temperature was increased to 1235 °C and held for a period of 30 min to achieve the decomposition of $SrCO_3$. During decomposition, an environment of 0.1 bar partial pressure of CO_2 was maintained with a 90 mL min^{-1} flow of argon alongside 10 mL min^{-1} of CO_2. This two-step procedure was repeated for a total of ten cycles per specimen. Upon completion of each experiment, specimens were allowed to cool to room temperature under inert gas flow. Immediately after cooling and removal from the TG, each specimen was weighed and measured using a Vernier caliper to estimate the volume. Specimens were then set in epoxy in preparation for imaging and to guard against potential hydration in air.

Acknowledgements

We would like to thank the U.S. Department of Energy SunShot Initiative for funding on award DE-EE0006534.

Keywords: concentrated solar power · energy storage · reactive stability · strontium oxide

[1] J. Stekli, L. Irwin, R. Pitchumani, *J. Thermal Sci. Eng. Appl.* **2013**, *5*, 021011.
[2] G. Ervin, *J. Solid State Chem.* **1977**, *22*, 51–61.
[3] R. Dunn, K. Lovegrove, G. Burgess, *Proc. IEEE* **2012**, *100*, 391–400.
[4] B. Wong, L. Brown, R. Buckingham, D. Thomey, M. Roeb, C. Sattler, *in SolarPACES 2012*, Marrakech, Morocco **2012**.
[5] D. N. Harries, M. Paskevicius, D. A. Sheppard, T. E. C. Price, C. E. Buckley, *Proc. IEEE* **2012**, *100*, 539–549.
[6] D. A. Sheppard, C. Corgnale, B. Hardy, T. Motyka, R. Zidan, M. Paskevicius, C. E. Buckley, *RSC Adv.* **2014**, *4*, 26552–26562.
[7] S. E. B. Edwards, V. Materic, *Sol. Energy* **2012**, *86*, 2494–2503.
[8] Y. Kato, T. O-shima, Y. Yoshizawa, *Int. J. Energy Res.* **2001**, *25*, 577–589.
[9] M. Kubota, K. Kyaw, F. Watanabe, H. Matsuda, M. Hasatani, *J. Chem. Eng. Jpn.* **2000**, *33*, 797–800.
[10] Y. Kato, D. Saku, N. Harada, Y. Yoshizawa, *J. Chem. Eng. Jpn.* **1997**, *30*, 1013–1019.
[11] M. S. Murthy, P. Raghavendrachar, S. V. Sriram, *Sol. Energy* **1986**, *36*, 53–62.
[12] R. Barker, *J. Appl. Chem. Biotechnol.* **1974**, *24*, 221–227.
[13] M. Aihara, T. Yoshii, Y. Shimazaki, T. Takeuchi, H. Habuka, *J. Chem. Eng. Jpn.* **2008**, *41*, 513–518.
[14] M. Zhao, J. Shi, X. Zhong, S. Tian, J. Blamey, J. Jiang, P. Fennell, *Energy Environ. Sci.* **2014**, *7*, 3291–3295.
[15] L. Reich, L. Yue, R. Bader, W. Lipinski, *Aerosol Air Qual. Res.* **2014**, *14*, 500–514.
[16] E. Mostafavi, M. H. Sedghkerdar, N. Mahinpey, *Ind. Eng. Chem. Res.* **2013**, *52*, 4725–4733.
[17] W. Liu, H. An, C. Qin, J. Yin, G. Wang, B. Feng, M. Xu, *Energy Fuels* **2012**, *26*, 2751–2767.
[18] S. P. Wang, S. L. Yan, X. B. Ma, J. L. Gong, *Energy Environ. Sci.* **2011**, *4*, 3805–3819.
[19] H. Chen, C. Zhao, Y. Li, X. Chen, *Energy Fuels* **2010**, *24*, 5751–5756.
[20] H. Chen, C. Zhao, W. Yu, *Appl. Energy* **2013**, *112*, 67–74.
[21] N. Rong, Q. Wang, M. Fang, L. Cheng, Z. Luo, K. Cen, *Energy Fuels* **2013**, *27*, 5332–5340.
[22] L. Rouchon, L. Favergeon, M. Pijolat, *J. Therm. Anal. Calorim.* **2013**, *113*, 1145–1155.
[23] Z. Zhou, Y. Qi, M. Xie, Z. Cheng, W. Yuan, *Chem. Eng. Sci.* **2012**, *74*, 172–180.
[24] F.-C. Yu, L.-S. Fan, *Ind. Eng. Chem. Res.* **2011**, *50*, 11528–11536.
[25] W. Liu, B. Feng, Y. Wu, G. Wang, J. Barry, J. C. D. da Costa, *Environ. Sci. Technol.* **2010**, *44*, 3093–3097.
[26] B. Yu, P. Zhang, L. Zhang, J. Chen, J. Xu, *Sci. China Ser. B* **2008**, *51*, 878–886.
[27] C. Qin, W. Liu, H. An, J. Yin, B. Feng, *Environ. Sci. Technol.* **2012**, *46*, 1932–1939.
[28] M. Valverde, P. E. Sanches-Jimenez, L. A. Perez-Maqueda, *Fuel* **2014**, *123*, 79–85.
[29] M. Kubota, K. Kyaw, F. Watanabe, H. Matsuda, M. Hasatani, *J. Chem. Eng. Jpn.* **2001**, *34*, 326–332.
[30] P. Wasserscheid, W. Arlt, German patent, DE 102010009543 .
[31] S. A. Robbins, R. G. Rupard, B. J. Weddle, T. R. Maull, P. K. Gallagher, *Thermochim. Acta* **1995**, *269*, 43–49.
[32] E. L. Charsley, C. M. Earnest, P. K. Gallagher, M. J. Richardson, *J. Therm. Anal.* **1993**, *40*, 1415–1422.
[33] A. M. Kierzkowska, R. Pacciani, C. R. Mueller, *ChemSusChem* **2013**, *6*, 1130–1148.
[34] S. Haussener, A. Steinfeld, *Materials* **2012**, *5*, 192–209.
[35] K. M. Allen, E. N. Coker, N. AuYeung, J. F. Klausner, *JOM* **2013**, *65*, 1670–1681.
[36] Z. Li, Y. Liu, N. Cai, *Chem. Eng. Sci.* **2013**, *89*, 235–243.
[37] L. Li, D. L. King, Z. Nie, C. Howard, *Ind. Eng. Chem. Res.* **2009**, *48*, 10604–10106.

Received: July 28, 2015
Published online on ■■ ■■, 0000

Sun off, storage on: A thermochemical energy storage (TCES) system based on a $SrO/SrCO_3$ carbonation cycle is investigated. The $SrCO_3/SrO$ systems supported by zirconia-based sintering inhibitors exhibit energy density exceeding 1500 $MJ\,m^{-3}$ for ten cycles at temperatures not previously approached by other TCES systems. The high-temperature nature of this TCES concept could potentially power a solar-driven combined cycle power plant at times of no solar input.

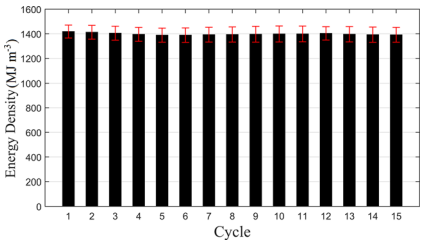

*N. R. Rhodes, A. Barde, K. Randhir, L. Li, D. W. Hahn, R. Mei, J. F. Klausner, N. AuYeung**

■■ – ■■

Solar Thermochemical Energy Storage Through Carbonation Cycles of $SrCO_3$/SrO Supported on $SrZrO_3$